Available online at www.sciencedirect.com
ScienceDirect
Computers and Structures 85 (2007) 977–987
Computers & Structures
www.elsevier.com/locate/compstruc

On the initial configurations of collapsible channel flow

Xiaoyu Luo *, Ben Calderhead, Haofei Liu, Wenguang Li

Department of Mathematics, University of Glasgow, Glasgow Q12 8QW, UK

Received 1 June 2006; accepted 21 November 2006
Available online 17 January 2007

Abstract

This paper studies the effect of the initial configurations of the governing equations on flows in a collapsible channel where the upper elastic wall is replaced by a pre-stretched beam. The aim is to check the existence of a "tongue" shaped neutral stability curve in the Reynolds number–tension space from a fluid-beam model [Luo XY, Cai ZX. Effects of wall stiffness on the linear stability of flow in an elastic channel. In: de Langre E, Axisa F, editors. Proceedings of the eighth international conference on flow-induced vibrations, FIV2004, vol. II. Paris, France: 2004. p. 167–70], in a properly formulated initial strain configuration. It was found that, for a given Reynolds number, as the tension is lowered to a critical value, the system becomes unstable, which is to be expected. However, a further decrease of the tension re-stabilizes the system before it becomes unstable again. It was possible that this puzzling finding was an artefact since the elastic equations used in the model were not properly derived from the zero initial stress configuration (Ogden, private communication). To check this, in this paper, a range of steady solutions are studied with both zero and non-zero initial wall tension. These are compared with the results using the finite element package Adina 8.3 using both the initial strain and initial stress configurations. As expected, the fluid-beam model agrees with Adina when using the initial stress configuration, but not when using the initial strain configuration. For cases with a small initial tension or small deformation (very large initial tension), both initial stress and initial strain configurations lead to very similar results, however, when the initial tension is comparable with the stretching induced tension, there are obvious differences in these two configurations. The "tongue" stability curve is then re-calculated with a zero initial tension, and re-plotted in the Reynolds number–effective tension space. It is interesting to see that though slightly different in shape, the "tongue" stable zone appears again when the zero initial tension is used. Thus it is highly likely that the puzzling "tongue" in the neutral stability curve is not due to the modelling approximation, but indicating a real, interesting physical phenomenon.

Keywords: Initial stress; Initial strain; Collapsible channel flow; Finite element methods; Neutral stability; Eigenvalue problem; Fluid–structure interactions

1. Introduction

Flow in collapsible tubes has been extensively studied in the last few decades, not only for its relevance to physiological applications, but also for the interesting fluid–structure interactions that occur in the system [2–12]. Self-excited oscillations in such a system are frequently observed in the laboratory in a "Starling resistor" [13,14]. Similar oscillations have also been reproduced using one-dimensional [15,16], or two-dimensional models [17–20]. Due to extensive computational requirements, to date except for steady or simplified simulations [21–23], there have been almost no reports on self-excited oscillations in truly three-dimensional models, which would be desirable to make full quantitative comparisons with experiments. However, it is believed that simple 1-D and 2-D models, though some based on rather crude approximations, can serve to shed light on many important features of the dynamics of the system.

The fluid-membrane model employed by Luo and Pedley [17–19], like other similar two-dimensional models of this type, suffers from several *ad hoc* approximations: the membrane was inextensible, the bending wall stiffness was ignored, and the elastic wall was assumed to move either

* Corresponding author. Tel.: +44 141 3304746; fax: +44 141 3304111.
E-mail address: x.y.luo@maths.gla.ac.uk (X. Luo).

0045-7949/$ - see front matter © 2006 Elsevier Ltd. All rights reserved.
doi:10.1016/j.compstruc.2006.11.010

in the vertical or in the normal direction. Although these may be adequate for steady flow simulations, their influence on unsteady flows, especially on the self-excited oscillations, needs to be carefully evaluated. Recently, a fluid-beam model in which the membrane is replaced by a plane strained elastic beam with large deflection has been put forward by Cai and Luo [24]. In this model the two-dimensional solid mechanics of the wall is taken into account, thus avoiding the above *ad hoc* assumptions. An ALE (Arbitrary Lagrangian Eulerian) solver combined with a method of rotating spines was used to solve the two-dimensional Navier–Stokes equations fully coupled with the two-dimensional non-linear large displacement structural equations [24]. Extending this model to study unsteady motions, Luo and Cai [1] discovered that the system gives rise to various different types of self-excited oscillations. It is found that the small amplitude oscillations are in excellent agreement with those predicted by solving the linearized Orr-Sommerfield equations of the system perturbed around the numerically simulated large deformation steady solutions. Most interestingly, they found an intriguing "tongue" shaped neutral stability curve in the Reynolds number-tension space, see Fig. 1.

This curve shows that, for a given Re, the beam is stable for a large value of the longitudinal initial tension, and unstable when the tension is below a certain level. However, inside the unstable zone when tension is lower than a critical value, there exists a tongue shaped zone when the system becomes stable again. As it seems bizarre that reducing the tension may re-stabilize the system, it is natural to ask if this is really physical or due to a flaw in the model. In fact, it is possible that this puzzling finding was an artifact, because the elastic equations used in the model were not properly derived from the zero initial stress configuration (we are grateful to Professor R.W. Ogden for pointing this out). The concept of the eigensolution of the system is essentially based on the energy arguments (the total energy must be minimum), which is only valid for solid equations derived from a zero initial stress configuration [25]. However in the fluid-beam model (as is commonly done by many other two-dimensional models), the initial stress approach is used [1,24]. In other words, does the "tongue" exist if the initial stress is free? This paper aims to answer this question and investigate the effects of the initial configurations on the steady solutions and on the neutral curve.

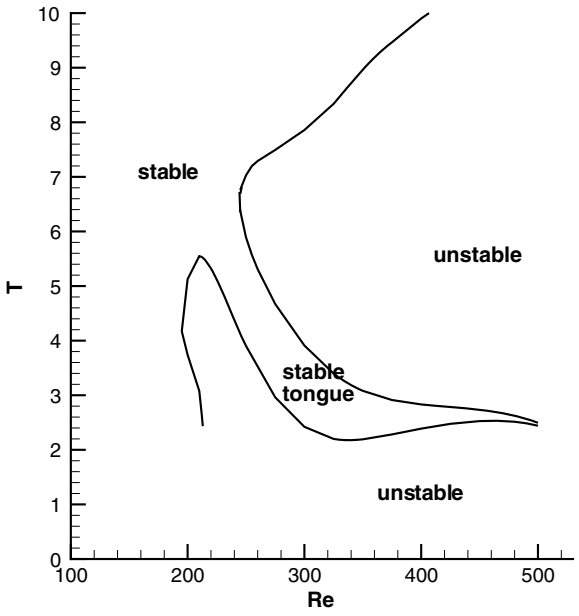

Fig. 1. The neutral stability curve in Re–T space predicted by [1] for $c_l = 600$, and $p_e = 1.95$ (see text for parameter definitions). Note there is a stability "tongue" sandwiched by the otherwise unstable regions.

2. The initial strain and initial stress configurations

The model consists of a steady flow in a channel in which a part of the upper wall is replaced by an elastic beam, see Fig. 2. The rigid channel has width D, a part of the upper wall with length L is replaced by a pre-stressed elastic beam subjected to an external pressure p_e. L_u and L_d are the lengths of the upstream and downstream rigid part of the channel. Steady Poiseuille's flow with average velocity U_0 is assumed at the entrance. The flow is incompressible and laminar, the fluid having density ρ and viscosity μ. The extensional and bending stiffness of the beam are EA and EJ, respectively, where E is the Young's modulus,[1] A is the thickness of the beam, and J is the bending moment. The pre-tension in the beam (caused by an initial stretch of the beam) is T and the density of the beam is ρ_m. Damping and rotational inertia of the beam are both neglected.

If the initial length of the elastic wall is l_0, see Fig. 3, and the length between the two rigid walls is l, then for zero initial stress, $l_0 = l$. The principal stretch is then defined as $\lambda = ds/dZ$. However, if there is an initial stretch, then $l_0 < l$, and

$$\lambda = \frac{ds}{dZ_0} = \frac{ds}{dZ}\frac{dZ}{dZ_0} = \lambda_x \lambda_0, \tag{1}$$

where $\lambda_x = ds/dZ$ is the stretch defined with l. It is important to realize that unless $\lambda_0 = 1$ (i.e. $Z_0 = Z$), $\lambda \neq \lambda_0 \neq \lambda_x$. If the principal stretch is defined with the initial length l_0, as in (1), this is known as the initial strain formulation. The other typical method used in solid mechanics is so called the initial stress formulation. In this formulation the principal stretch is defined with the deformed length l, i.e., λ_x, rather than λ, is used. However to account for the effect of the initial deformation, an initial stress σ_0 $(=T/A)$ is added to the stress in the governing equations. Note, the initial strain formulation is defined with the initial zero stress configuration. The stretching energy for this case can be written as

[1] As, we consider a plane strain problem here, E here is equivalent to the conventional Young's modulus divided by $(1 - \nu^2)$, where ν is the Poisson's ratio.

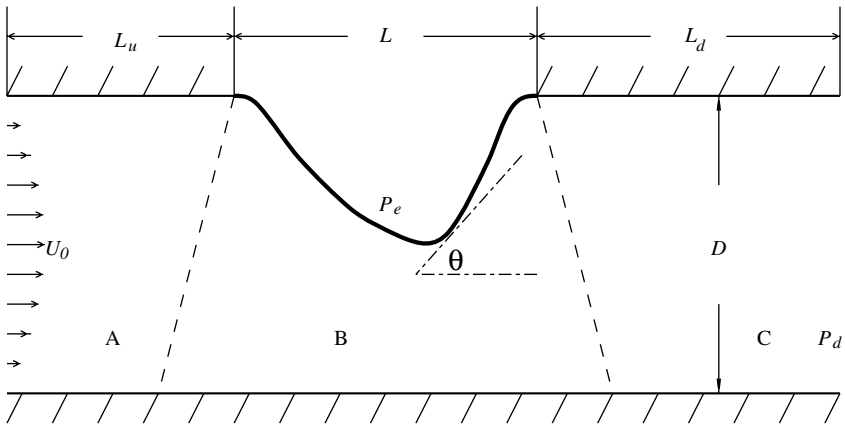

Fig. 2. The flow-beam configuration (not to scale). Part B has part of the wall being replaced by an elastic beam.

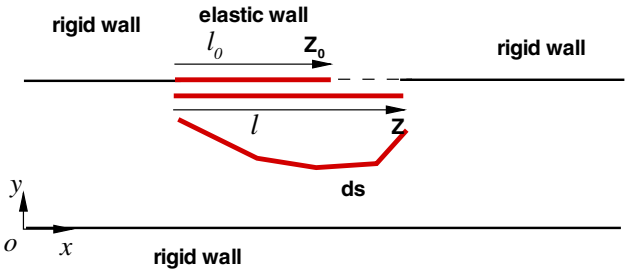

Fig. 3. Definition of the initial configurations.

$$\frac{1}{2}c_\lambda(\lambda-1)^2=\frac{1}{2}c_\lambda(\lambda_0\lambda_x-1)^2. \tag{2}$$

On the other hand, the initial stress configuration is only an approximation of the original problem and its stretching energy is $\frac{1}{2}c_\lambda(\lambda_x-1)^2$, which is not the same as (2) unless $\lambda_0=1$. However, this formulation is commonly used in many previous models [8,9,17–19]. In addition, it is often assumed that the tension is constant along the elastic wall, i.e., the additional tension induced by deformation and fluid stresses is negligible, thus $\lambda=\lambda_0=$ constant. Some models also assumed that the wall moves only in the y-direction [26,27]. These are all valid approximations provided the wall deformation is small. However, for large deformation, non-linear, problems, if the stability analysis is carried out on an eigenproblem which is based on energy argument, it is important that the strain energy is calculated using the principal stretch defined by Eq. (1) [25], in other words, the initial strain formulation should be employed.

The strategy of the study is as follows. First, the results from the fluid-beam model will be compared with that of the commercial finite element package Adina 8.2, for the same model problem, using both the initial stress and initial strain configurations. The differences between these results will be discussed. Then the neutral curve for the problem with a zero initial tension will be computed, as this implies that $\lambda=\lambda_x$ ($\lambda_0=1$). This new neutral curve will then be compared with the old curve, in order to identify the existence of the "tongue".

3. Governing equations

3.1. The governing equations for the fluid-beam model

For convenience, the flow velocity components u_i, fluid stresses σ_i, pressure p, time t, the Cartesian coordinates x, y (originated at the left bottom of the channel), and length l are non-dimensionlized as follows:

$$u_i^*=\frac{u_i}{U_0},\quad \sigma_i^*=\frac{\sigma_i}{\rho U_0^2},\quad p^*=\frac{p}{\rho U_0^2},\quad t^*=\frac{tU_0}{D},$$
$$l^*=\frac{l}{D},\quad x^*=\frac{x}{D},\quad y^*=\frac{y}{D},\quad (i=1,2), \tag{3}$$

where the non-dimensional parameters, such as the initial tension T, the curvature κ, the density of the beam ρ_m, the wall stiffness EA, EJ, and the Reynolds number are similarly scaled as

$$T^*=\frac{T}{\rho U_0^2 D},\quad \kappa^*=\kappa D,\quad \rho_m^*=\frac{h\rho_m}{\rho D},\quad c_\lambda=\frac{EA}{\rho U_0^2 D},$$
$$c_\kappa=\frac{EJ}{\rho U_0^2 D^3},\quad Re=\frac{U_0 D\rho}{\mu}. \tag{4}$$

The variables with a star are the non-dimensional ones, which will be used throughout this paper. In the following, however, the stars are dropped for simplicity.

Note c_λ and c_k are not independent to each other, and they are related by

$$c_\kappa=c_\lambda\frac{A^2}{12D^2}. \tag{5}$$

We define the principal stretch $\lambda=\sqrt{x'^2+y'^2}$ and wall curvature $\kappa=\frac{x'y''-y'x''}{\lambda^3}$, where $x=x(l,t)$, $y=y(l,t)$, l is the x coordinate in the undeformed configuration, and the prime denotes differentiation with respect to l. Using the Kirchhoff constitutive laws for the elastic beam, and dropping the stars for convenience, we write the dimensionless governing equations for the beam (for derivation of these, see [24]):

$$\frac{\rho_m}{\lambda}\left(x'\frac{d^2x}{dt^2}+y'\frac{d^2y}{dt^2}\right)=c_\kappa\kappa\kappa'+c_\lambda\lambda'+\lambda\tau_n=0, \tag{6}$$

$$\frac{\rho_m}{\lambda}\left(y'\frac{d^2x}{dt^2}-x'\frac{d^2y}{dt^2}\right)=c_\kappa\left(\frac{1}{\lambda}\kappa'\right)'-\lambda\kappa T-c_\lambda\lambda\kappa(\lambda-1)-\lambda\sigma_n+\lambda p_e=0, \tag{7}$$

$$x'=\lambda\cos\theta,\quad y'=\lambda\sin\theta,\quad \theta'=\lambda\kappa. \tag{8}$$

And the fluid flow obeys the Navier–Stokes equations:

$$\frac{\partial u_i}{\partial t}+u_j u_{i,j}=-p_{,i}+\frac{1}{Re}u_{i,jj}, \tag{9}$$

$$u_{i,i}=0,\quad i,j=1,2, \tag{10}$$

where θ is the rotating angle of the beam in the horizontal position, σ_n and τ_n are the normal and shear stresses of fluid on the beam which can be expressed as

$$\sigma_n=p-\frac{2}{Re}\frac{\partial u_n}{\partial n},\quad \tau_n=-\frac{1}{Re}\left(\frac{\partial u_s}{\partial n}+\frac{\partial u_n}{\partial s}\right), \tag{11}$$

where s and n indicate the tangential and the normal direction of the beam. Note that as both c_κ and $c_\lambda\to 0$, we recover the fluid-membrane model [8].

Boundary conditions for the flow field are chosen such that steady parabolic velocity profile is used for the upstream inlet, the stress free condition is used for the downstream outlet, and the no-slip condition is used along the walls including the elastic section. Clamped conditions are used for the two ends of the beam.

It is important to note that on deriving (6) and (7), the initial stress configuration is used, i.e., all deformations are defined with the length L in Fig. 3, thus $\lambda=\lambda_x$, and the initial stress is $\sigma_0=T/A$.

3.2. The Adina models

To compare our results with Adina (version 8.2), we rebuild the fluid-beam configuration (Fig. 2) using Adina's fluid structure interaction solver [28]. The governing equations for the fluid are the same as Eqs. (9) and (10). For the structure, we solve a plane strain problem (as in the fluid-beam formulation); only a slice of structure with unit thickness is considered, and all strain components in z-direction are zero. Thus the governing equation is derived from the principle of virtual work:

$$\int_V \tau_{ij}\delta e_{ij}dV=\int_S f^s\delta u^s dS\quad i,j=1,2, \tag{12}$$

where τ_{ij} is the Cauchy stress tensor, e_{ij} is the strain tensor corresponding to virtual displacements, and V is the volume, S is the surface on which external traction (pressure) f^s is applied, and δu^s are the components of virtual displacement vector evaluated on the surface S. When there is an initial tension, this can be specified with the initial strain approach, i.e., an initial strain, e_{11}, in the x-direction is added to the strain tensor e_{ij}, which is defined with the initial resting length of the beam, l_0. Alternatively, this can be specified with the initial stress approach, i.e., the initial stress $\sigma_{11}=\frac{T}{A}$ is added to the stress tensor σ_{ij}, and e_{ij} is now defined with the length l [28].

For the two-dimensional beam, (12) is evaluated with a unit length in z-direction, and can be written as [30]

$$EJ\int\frac{d\beta}{dx}\frac{d\delta\beta}{dx}dx+GSk\int\left(\frac{dw}{dx}-\beta\right)\left(\frac{d\delta w}{dx}-\delta\beta\right)dx=\int f\delta w dx+\int m\delta\beta dx, \tag{13}$$

where f and m are the transverse and moment loadings per unit length, EJ is the wall stiffness, w and β are the displacement and total rotation of the mid-plane which is assumed to remain a plane after deformation. G is the shear modulus, S is the cross-sectional area, and k is a shear constant which is 5/6 for a rectangular cross-section [29]. Note the second term in (13) represents the shear effect [29], which is considered to be small for a thin beam and is ignored in our formulation [24]. Note if the initial stress approach is used, the final equations Adina solves is almost identical (except the shear effect) to the fluid-beam model, thus the results from these two models should be the more or less the same. However, if the initial strain configuration is used, then these two formulations are different unless the initial strain is zero (i.e. $\lambda_0=1$). Results from both initial configurations will be computed and compared with those from the fluid-beam model.

4. Numerical methods

4.1. Numerical methods for the fluid-beam model

A finite element code for unsteady flow is developed to solve the coupled non-linear fluid–structure interactive equations simultaneously, and an adaptive mesh with rotating spines is used to allow for a movable boundary. The mesh is divided into three subdomains, one of which is placed with many spines originating from the bottom rigid wall to the movable beam [24]. These spines are straight lines, which can rotate around the fixed nodes at the bottom. Thus all the nodes on the spines can be stretched or compressed depending on the beam deformation. A numerical code is developed to solve the fluid and the beam equations simultaneously using weighted residual methods.

A Petrov–Galerkin method is used to discretise the system Eqs. (6)–(10). The element type for flow is 6-node triangular with second order shape function N_i for u and v, and linear shape function L_i for p. Three-node beam elements with second order shape function are used for x, y, θ, λ and κ. The discretised finite element equations can be written in a matrix form as

$$M(U)\frac{dU}{dt}+K(U)U-F=R=0, \tag{14}$$

where $U=(u_j,v_j,p_j,x_j,y_j,\theta_j,\lambda_j,\kappa_j)$ is the global vector of unknowns, and $j=1,\ldots n$, is the nodal number. **R** is the overall residual vector denoted by

$$\mathbf{R} = (R_x, R_y, R_c, R_{ex}, R_{ey}, R_{e\lambda}, R_{e\kappa}), \quad (15)$$

where the subscripts x, y, c indicate the corresponding residuals of the x and y-momentum and continuity in fluid, and $e_x, e_y, e_\theta, e_\lambda, e_\kappa$ indicate the corresponding residuals of Eqs. (6)–(10).

An implicit finite difference second order predictor-correct scheme with a variable time step is used to solve the time dependent problem. At each time step, the frontal method and a Newton–Raphson scheme are employed to obtain the converged solution for the whole system simultaneously.

4.2. Numerical accuracy for the fluid-beam model

Validations for the fluid-beam model have been performed extensively where a grid size ratio was given based on the boundary thickness [24]. In this study, two different grids are used. Grid B, the coarser one, where only $16 \times (20 + 60 + 60)$ elements are used with the stretch ratio of 1:10 towards the corners, is initially used for all simulations. Grid A, a more refined one, which can solve for the smallest value of the extensional stiffness parameter is used to rerun the steady and unsteady simulations when large deformation occurs. In this case, the smallest boundary layer width is estimated to be about 0.0141, and the grid is chosen to be $22 \times (70 + 120 + 200)$ with the same stretch ratio towards the two corners where the beam joins the rigid wall in both directions. The computations are performed on Euclid2, a twin PentiumIV processors (3.4 GHz) Linux machine with 8GB memory at Glasgow University, and take about 0.1–1 CPU min for a typical steady solution.

4.3. Numerical methods for Adina model

Here we solve a large deformation, small strain problem by using a total lagrange formulation [30]. For the elastic wall, 3-node isoparametric beam elements are used, which allows for large displacement with small strains, and 3-node triangle elements are used for the fluid (as Adina 8.3 do not have 6-node triangle fluid element). A typical mesh used is shown in Fig. 4.

A movable mesh was used over the fluid domain, so as to increase the accuracy of the calculations as the flexible wall moved.

The finite element equations for the coupled fluid–structure system are derived from the Pertov–Galerkin variational formulation, which are solved using either an iterative or a direct approach [30]. For the iterative method, the fluid and structural domains are treated separately, using the most recent solution for one domain to obtain the solution for the other domain. These iterations are carried out until the coupled equations were satisfied. For the direct method, the fluid and structural equations are combined into a matrix system of equations and solved simultaneously. The direct method requires more memory, but is faster than the iterative method. However, in cases where the beam deformation was large, the direct method fails to give convergence and the iterative approach has to be used. Solutions of the matrix equations are obtained using a sparse matrix direct solver based on Gaussian elimination [28].

Results for steady simulations are obtained starting with an initially undeformed channel, with the flexible beam aligned with the upper channel wall. Because of difficulties in obtaining converged solutions due to the non-linearities associated with large beam deformations, it was necessary to apply the inlet flow and the external pressure incrementally. This minimized any element distortion normally associated with rapid mesh deformation.

4.4. Numerical accuracy for Adina model

In order to verify the grid independence, meshes with different numbers of elements were used and the results compared. These verification studies were carried out with zero pre-tension in the beam and for the Young's modulus of 35.89 kPa, and $c_\lambda = 500$. Each mesh was checked by increasing the grid points of previously tested mesh. This was continued until the changes of both the maximum displacement of the beam and the maximum pressure in the flow domain are within 0.5% between different meshes. These results were also verified by comparing them to the results obtained by Luo and Pedley [8]. The mesh eventually used had 26,839 elements.

5. Results

5.1. Parameters

Following [24], the dimensionless parameters are chosen to be

$$Re = 300, \quad D = 1, \quad L_u = 5, \quad L = 5, \quad L_d = 30, \quad p_e = 1.95,$$
$$\rho_m = 0, \quad c_\lambda = 1 - 1000, \quad A/D = 0.01 - 0.1, \quad T_0 = 178.8,$$

where $\beta(>0)$ was used by Luo and Pedley [17] to scale tension: $T = T_0/\beta$. When $\beta \to \infty$, $T = 0$. A/D is the ratio between the beam wall thickness and the channel height.

Fig. 4. A typical mesh for the deformed system in the Adina model.

The required input parameters for Adina are the inlet velocity U_0, the external pressure P_e, the initial strain ε, the Young's modulus E, the channel depth, and the wall thickness A. These can be obtained from our dimensionless parameters as follows:

$$U_0 = \frac{Re \times \mu}{\rho \times D}, \quad P_e = p_e \rho U_0^2, \quad E = \frac{c_\lambda \rho U_0^2 D(1-v^2)}{A},$$
$$T = (T_0/\beta) \times \rho U_0^2 D, \quad \varepsilon = \frac{T}{EA}, \tag{16}$$

where the Poisson's ratio v is chosen to be 0.45, density of fluid ρ is 1000 kg/m^3, the viscosity of fluid μ is 0.001 Pa s, the channel height D is 0.01 m, and the channel depth (in z-direction) is 1 m. For example, when $Re = 300$, $p_e = 1.95$, $c_\lambda = 1000$, $\beta = 90$, and $A/D = 0.01$, (16) gives

$$U_0 = 0.03 \text{ m}, \quad Pe = 1.755 \text{ Pa}, \quad E = 71.775 \text{ kPa},$$
$$A = 0.0001 \text{ m}, \quad \varepsilon = 0.0024911.$$

5.2. Effects of initial strain and initial stress configurations

First, consider a thin wall and choose $c_\kappa = 10^{-5} c_\lambda$, i.e., A is about 1% of the channel height. The computed elastic wall shapes for $c_\lambda = 200$, 500 and 1000, and different values of the initial tension (indicated by the values of β) are shown in Figs. 5a–c.

For $T = 0$ ($\beta = \infty$), all three approaches (fluid-beam model, Adina initial stress, Adina initial strain) give the same results for $c_\lambda = 500$, and $c_\lambda = 1000$. However, some differences are observed when $c_\lambda = 200$ between our results and that of Adina. This is presumably because Adina considered the shear effect, which is absent in our model. When the stretching stiffness is smaller, the shear effect becomes more significant. Therefore the deformation predicated by Adina is slightly smaller. However, in general, our fluid-beam model agrees very well with Adina when the initial stress configuration is used.

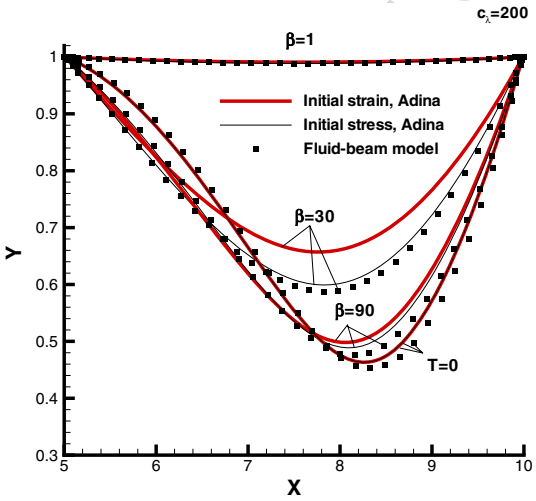

Fig. 5a. The elastic wall shapes for $c_\lambda = 200$, and $\beta = 1, 30, 60, 90, \infty$ ($T = 0$). The thicker solid lines are results from Adina with initial strain, and the thinner solid lines are from Adina with initial stress. The symbols are from the fluid-beam model.

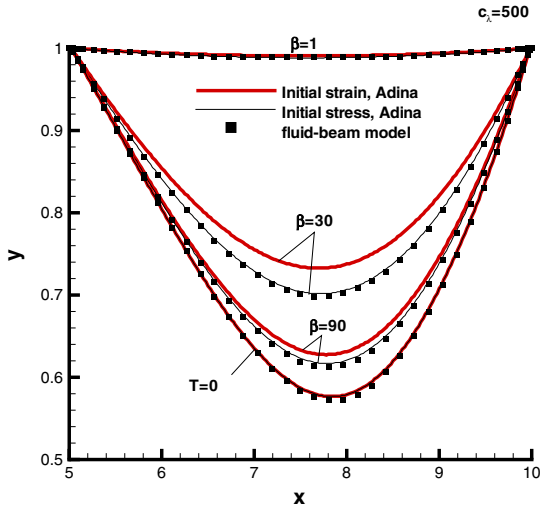

Fig. 5b. As in Fig. 5a, but for $c_\lambda = 500$.

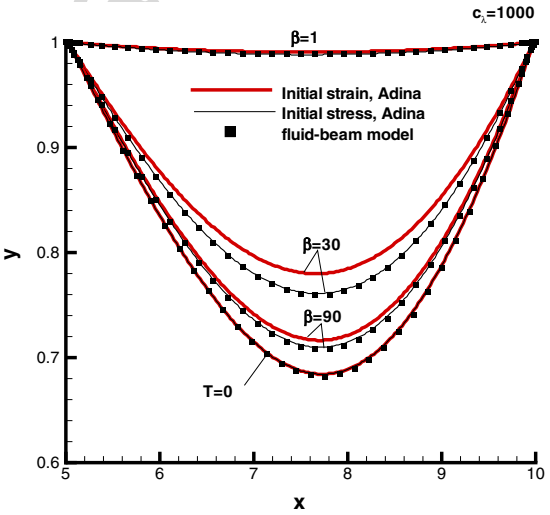

Fig. 5c. As in Fig. 5a, but for $c_\lambda = 1000$.

Now we compare the results using the initial stress (Adina and fluid-beam) and initial strain (Adina) configurations. When $T = 0$, these two configurations give identical results for all values of c_λ studied (at least for Adina). Interestingly, the results between the initial stress and initial strain approaches start to differ as the initial tension is increased, in both cases $\beta = 30$, and 90, the initial strain approach gives less deformation compared with that of the initial stress configuration. However, for $\beta = 1$ (i.e. the tension is very high), as the total deformation is now small, the differences between these two configurations become less obvious again. Thus for small deformation, the choice of the initial configurations is less important. This justifies the results from many previous studies using the initial stress approach. However, for large deformation, the difference between these two configurations is noticeable.

The corresponding streamlines and pressure contours predicted by both Adina (with the initial strain configuration) and the fluid-beam model are shown in Figs. 6 and 7 for $c_\lambda = 500$, and $c_\lambda = 1000$, respectively. It can be seen that the results are again similar (though the scaling is not exactly the same as these plots are output from two different software). The strength and range of the flow re-circulation is predicted by both models (though the fluid-beam model has less smooth stream functions due to the simple interpolations used). As the fluid-beam model gives slightly greater wall deformation (see Figs. 5b and c), this is reflected in the pressure field especially underneath the maximum deformation of the wall. The shaded semi-circle area (indicating the lowest pressure zone) is also larger in the fluid-beam model than in the Adina model. This is more obvious for $c_\lambda = 500$, as the differences in initial stress and initial strain configurations must be greater for lower values of c_λ.

5.3. The wall thickness effect

As all our previous results are obtained for a very thin wall thickness ($A \approx 1\%$), it is constructive to provide a set of solutions for different values of wall thickness. In doing so, we keep the Young's modulus E fixed (=35.9 kPa), and vary the wall thickness A from 1%, to 2%, 4%, 6%, 8% and 10% of the channel height, respectively. This implies that in the fluid-beam model, both c_λ and c_κ are changed

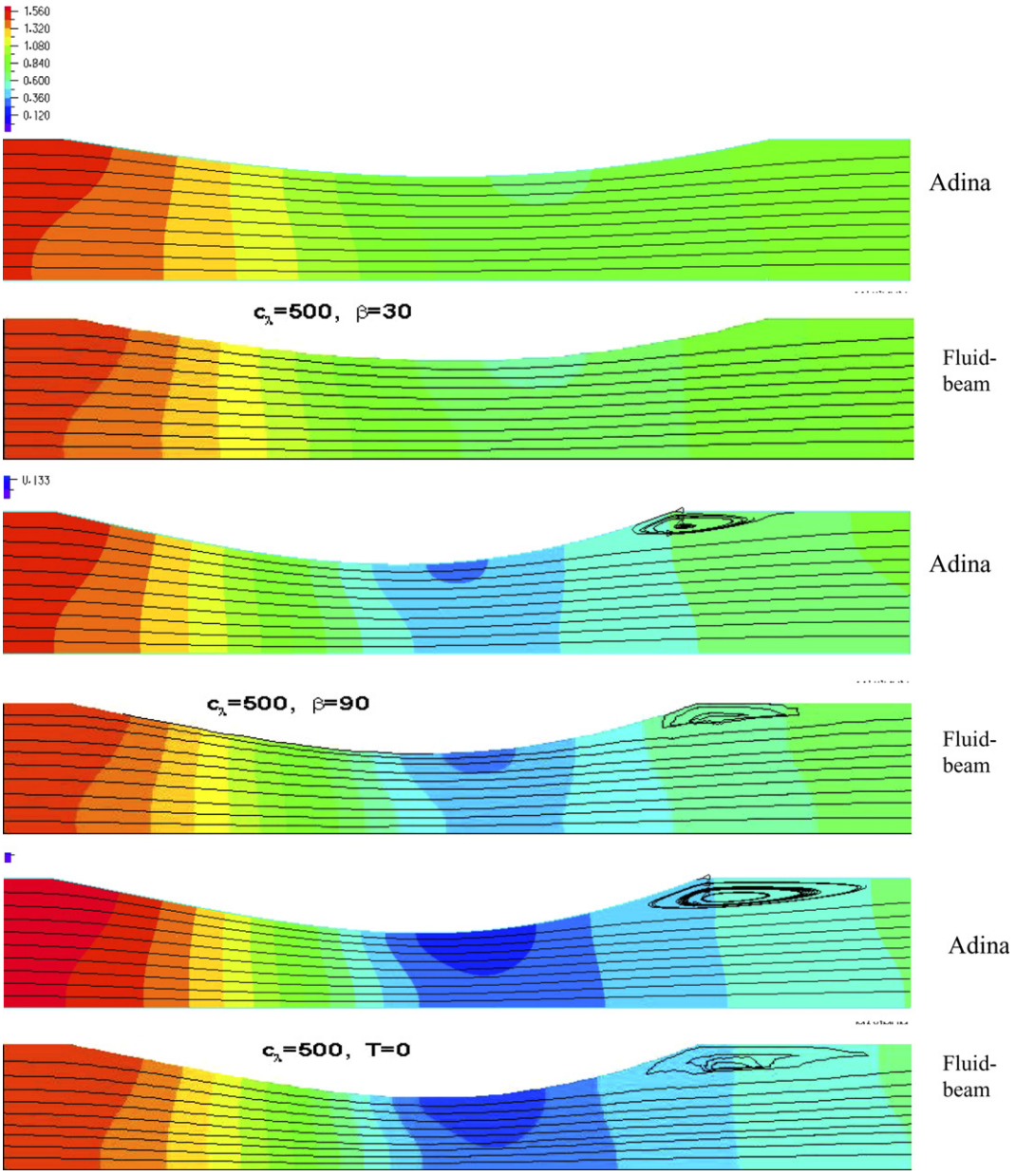

Fig. 6. Streamlines for $c_\lambda = 500$, and $\beta = 30$, 60 90, and $T = 0$. Overlapped are the corresponding pressure contours with bright colour indicating the higher pressure contour values.

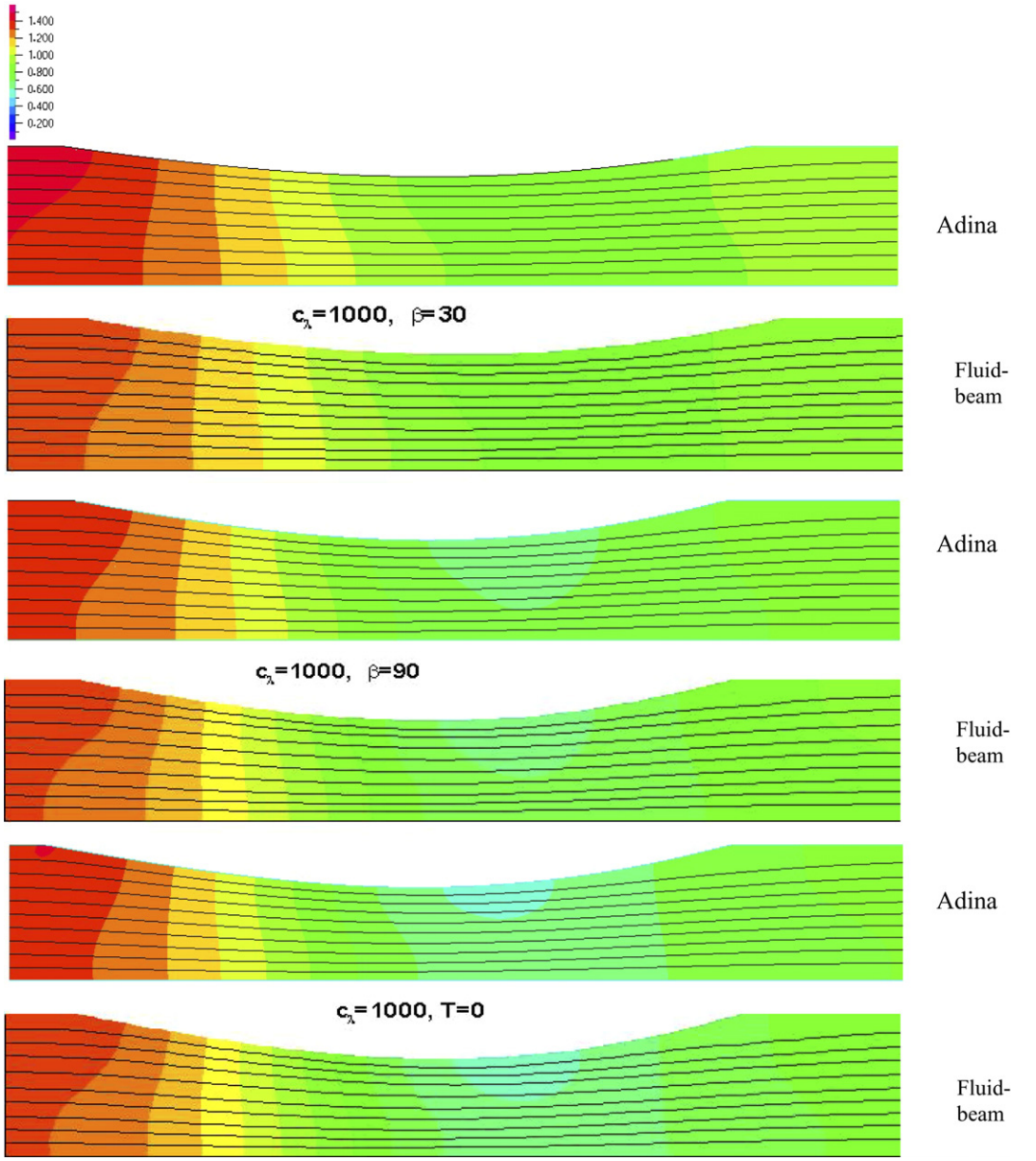

Fig. 7. Streamlines for $c_\lambda = 1000$, and $\beta = 30$, 90, and $T = 0$. Overlapped are the corresponding pressure contours with bright colour indicating the higher pressure contour values.

accordingly, see Eqs. (16) and (5), (e.g. $c_\lambda \approx 500$ for $A = 1\%$). The elastic wall shapes thus obtained are shown in Fig. 8. The solid curves are from Adina with the initial strain configuration, and the symbols are from the fluid-beam model. Again, the agreement between the two models for $T = 0$ is excellent.

The same results are shown in Fig. 9 but with an initial tension, $\beta = 30$. The differences between these two models (Adina uses the initial strain configuration and fluid-beam uses the initial stress configuration) become less and less noticeable as the wall thickness is increased from 1% to 10%. This is because the corresponding values of c_λ are greater in the thicker walled beam, and the initial tension chosen becomes less dominant compared with the stretch induced tension.

6. Discussions

We have successfully re-produced all our results using Adina with initial stress formulation. Initial stress approach is commonly used in many engineering applications where the previous loading history is unknown. However, the initial strain approach is defined more rigorously in the sense that all equations are derived from the zero initial stress configurations. Thus when the eigenvalue problem is solved [1], it may be essential that the initial strain configuration is used.

The key finding is that although the differences from these two initial configurations are small for the collapsible channel with small deformation, there are sufficient changes in the steady solutions using these two configura-

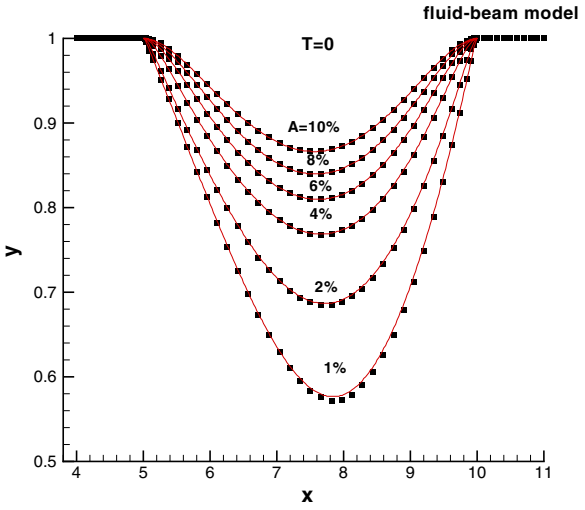

Fig. 8. Elastic wall shapes for different wall thickness obtained from the fluid-beam (symbols) and Adina initial strain (solid line), all with Young's modulus $E = 35.9$ kPa, and $T = 0$.

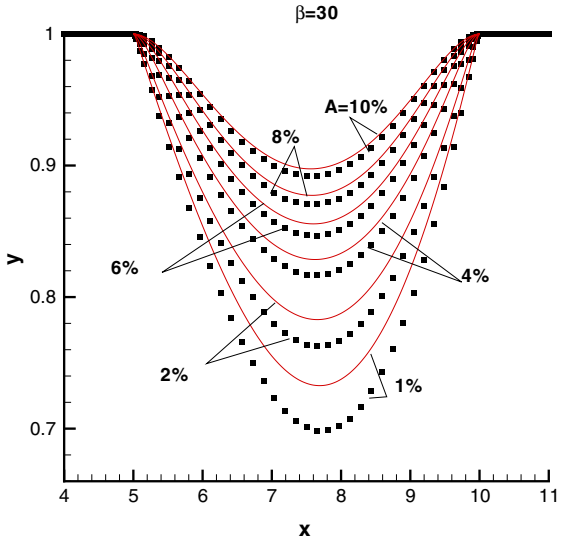

Fig. 9. As in Fig. 8, but with $\beta = 30$.

tions when the deformation is larger. These could lead to different results in the stability analysis, as the basic flow is slightly changed.

To make sure that the initial configuration is not responsible for the "tongue" observed in the neutral stability curve, we re-solve the eigenvalue problem with a zero initial tension, and then see if the "tongue" still occur. Note that in order to compare the new results with Fig. 1, we need to use the concept of the effective tension, which is defined as [24]:

$$T_{\text{eff}} = T_0 + c_\lambda(\lambda - 1), \tag{17}$$

where λ is the principal stretch ($=\lambda_x$) defined in Section 3.1. Since the principal stretch λ varies along the beam, we need to estimate the effective tension by calculating λ at a fixed station along the beam, say at the downstream end (calculating λ at any other position does not change the results significantly).

We would like to emphasis that the introduction of the effective tension is essential here since our new results are obtained for a zero initial tension. As defined in Eq. (17), the effective tension is the measure of the real tension that the beam experiences, whether or not the initial tension is zero. In the earlier study where the "tongue" was found, the initial tension was not zero. The use of the effective tension makes the two cases comparable. In other words, we need to plot both the neutral stability curves in the Re–T_{eff} space. Thus in scenario A, we prescribe T_0 and replot the neutral curve from Fig. 1 in the Re–T_{eff} space, and in scenario B, we let $T_0 = 0$, but adjust c_λ so that a same value of T_{eff} can be calculated from (17). All other parameters are kept to be the same. The results are shown in Fig. 10. For details of the eigenvalue problem, see [1,31].

It is highly interesting to see that although the new neutral curve (solid) is shifted downwards slightly in the Re–T_{eff} space (partly due to the small differences in basic flows using different initial configurations, and partly due to the fact that a finer mesh is used for the new results in the eigensolver), the two curves are very similar, both present the same qualitative features, i.e., both have the "tongue" structure. The first implication of this is that the concept of the effective tension is robust, and can be used as a key control parameter for the system. The other, more important observation, is that the "tongue" still exists, showing that it is not due to the fact the initial stress configuration was used.

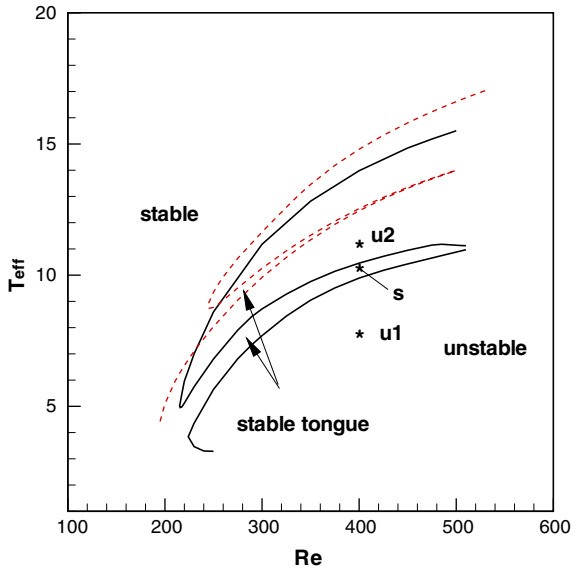

Fig. 10. The neutral stability curves in the Re–T_{eff} space . The solid curve is the new results obtained with a zero initial tension, while the dashed one is the one corresponding to Fig. 1. The three points $u1$, s, and $u2$ have the corresponding coordinates of $Re = 400$, and $T_{\text{eff}} = 7.67$, 10.19, and 8.45 ($c_\lambda = 310$, 380 and 500), respectively.

It may be said that a better way to check the tongue's existence is to simply run the unsteady simulations, and see if the solutions around this zone present same behaviour as predicted by Fig. 10. However, care should be taken here as the unsteady simulations are also obtained from the governing equations based on the initial stress configurations (unless T is zero), thus may suffer the same problem. Now that we have obtained the new neutral curve, we can run the unsteady simulations with the zero initial tension. Take the points $u1$, s, and $u2$ in Fig. 10, for example. If the tongue is true, then the unsteady solutions at $u1$, and $u2$ should be unstable, while at point s it should be stable. To obtain these solutions, an initial perturbation is applied to the corresponding steady solutions at these points, and the time response of the system is obtained. The results are shown in Fig. 11. The wall displacement in the y-direction at the mid-point of the beam initially is plotted against time. It is seen that the solution at s is indeed stable, as the perturbation decays with time. The solution at $u2$ it is indeed unstable, and the self-excited oscillation is developed and is growing with time. However, from the unsteady simulation it is harder to see that if solution at $u1$ is unstable or not in the longer term, since its growth rate seems to be very small. This is presumably because it is closer to the neutral curve than $u2$. It is for this reason, we could not use the unsteady simulations alone to determine the neutral curve, as on the neutral curve, all solutions have a zero growth rate, and an infinitely long time would be required to determine the growth rate. However, it is encouraging that the unsteady simulations support the existence of the tongue.

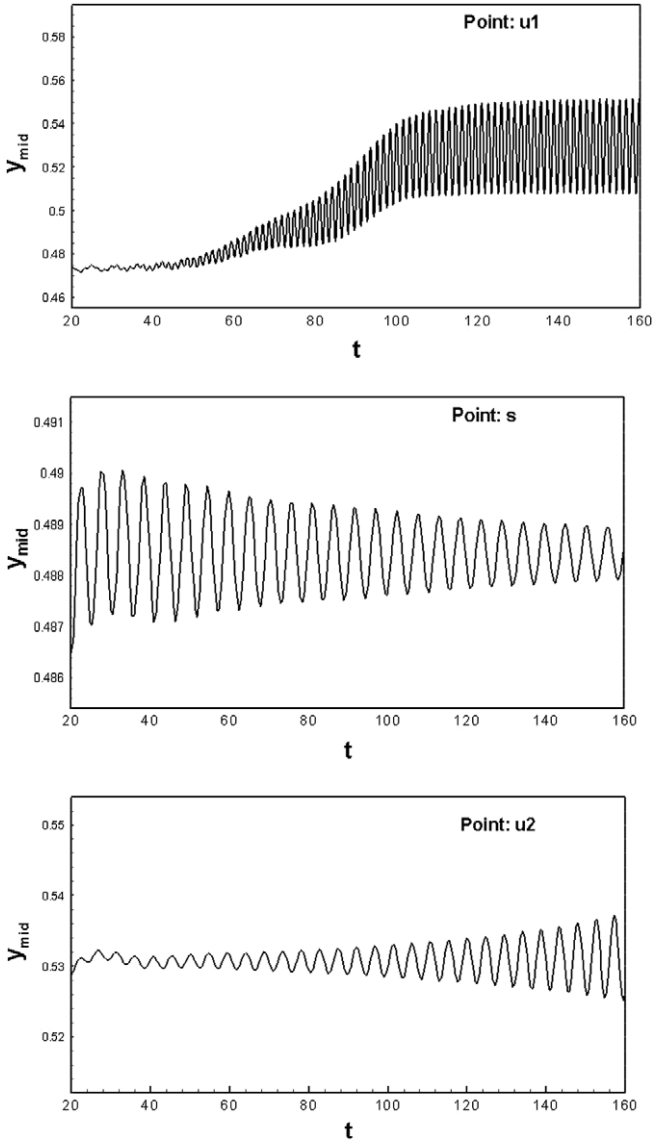

Fig. 11. The unsteady solutions at the three points $u1$, s, and $u2$ across the tongue zone, as shown in Fig. 10. Plotted is the y-displacement initially at the middle point of the beam against time.

7. Conclusions

The effects of the initial configurations on the steady solutions and the neutral stability curve of flow in collapsible channel are studied in this paper. Two independent numerical models are employed. One is the fluid-beam model [24]; the other is the iso-beam model (with a fluid–structure interaction solver) from the Adina with both the initial strain and initial stress configurations. As expected, the fluid-beam model agrees very well with Adina for the initial stress configuration; however, they differ when the initial strain configuration is used. The differences in the steady solutions between these two configurations are small if either the deformation is very small (tension is large) or the initial tension is small compared with the stretched induced tension. However, when these conditions are not met, there are some discrepancies between these two, suggesting that the principal stretch needs to be defined properly with the (zero-stressed) initial length. The most important finding is that we found that the same stability "tongue" exists in the Reynolds number-effective tension space, regardless of the initial configuration used. This is also supported by the full unsteady numerical simulations. Thus although a complete physical explanation of the "tongue" remains to be found, this work suggests that the "tongue" presents a real and interesting physical phenomenon.

Acknowledgements

This work is supported by the EPSRC (Grant No. GR/M07243) and the Royal Society of London (2005/R4-JP). Special thanks to Prof. R. Ogden and Prof. ZX Cai for useful discussions.

References

[1] Luo XY, Cai ZX. Effects of wall stiffness on the linear stability of flow in an elastic channel. In: de Langre E, Axisa F, editors. Proceedings of the eighth international conference on flow-induced vibrations, FIV2004, vol. II. Paris, France: 2004, p. 167–70.

[2] Shapiro AH. Steady flow in collapsible tubes. ASME J Biomech Eng 1977;99:126–47.
[3] Grotberg JB, Gavriely N. Flutter in collapsible tubes: a theoretical model of wheezes. J Appl Physiol 1989;66:2262–73.
[4] Kamm RD, Pedley TJ. Flow in collapsible tubes: a brief review. ASME J Biomech Eng 1989;111:117–79.
[5] Jensen OE, Pedley TJ. The existence of steady flow in a collapsed tube. J Fluid Mech 1989;206:339–74. 623–59.
[6] Matsuzaki Y, Fujimura K. Reexamination of steady solutions of a collapsible channel conveying fluid, a technical brief. ASME J Biomech Eng 1995;117:492–4.
[7] Grotberg JB. Pulmonary flow and transport phenomena. Annu Rev Fluid Mech 1994;26:529–71.
[8] Luo XY, Pedley TJ. A numerical simulation of steady flow in a 2D collapsible channel. J Fluids Struct 1995;9:149–74.
[9] Pedley TJ, Luo XY. Modelling flow and oscillations in collapsible tubes. Theor Comp Fluid Dyn 1998;10:277–94.
[10] Davies C, Carpenter PW. Instabilities in a plane channel flow between compliant walls. J Fluid Mech 1997;352:205–43.
[11] Davies C, Carpenter PW. Numerical simulation of the evolution of Tollmien–Schlichting waves over finite compliant panels. J Fluid Mech 1997;335:361–92.
[12] Heil M. Stokes flow in collapsible tubes: computation and experiment. J Fluid Mech 1997;353:285–312.
[13] Bertram CD. Two modes of instability in a thick-walled collapsible tube conveying a flow. J Biomech 1982;15:223–4.
[14] Bertram CD, Raymond CJ, Pedley TJ. Mapping of instabilities for flow through collapsed tubes of differing length. J Fluid Struct 1990;4:125–53.
[15] Jensen OE. Instabilities of flow in a collapsed tube. J Fluid Mech 1990;220:623–59.
[16] Jensen OE. Chaotic oscillations in a simple collapsible tube model. ASME J Biomech Eng 1992;114:55–9.
[17] Luo XY, Pedley TJ. A numerical simulation of unsteady flow in a 2D collapsible channel. J Fluid Mech 1996;314:191–225.
[18] Luo XY, Pedley TJ. The effects of wall inertia on flow in a 2-D collapsible channel. J Fluid Mech 1998;363:253–80.
[19] Luo XY, Pedley TJ. Flow limitation and multiple solutions in 2-D collapsible channel flow. J Fluid Mech 2000;420:301–24.
[20] Jensen OE, Heil MH. High frequency self-excited oscillations in a collapsible-channel flow. J Fluid Mech 2003;481:235–68.
[21] Hazel AL, Heil MH. Steady finite-Reynolds-number flows in three-dimensional collapsible tubes. J Fluid Mech 2003;486:79–103.
[22] Marzo A, Luo XY, Bertram CD. Three-dimensional flow through a thick-walled collapsible tube. J Fluid Struct 2005;20:817–35.
[23] Heil M, Waters SL. Transverse flows in a rapidly oscillating, elastic cylindrical shells. J Fluid Mech 2006;547:185–214.
[24] Cai ZX, Luo XY. A fluid-beam model for flow in a collapsible channel. J Fluid Struct 2003;17:125–46.
[25] Steigmann DJ, Ogden RW. Plane deformations of elastic solids with intrinsic boundary elasticity. Proc R Soc London A 1997;453:853–77.
[26] Carpenter PW, Garrard AD. The hydrodynamic stability of flow over Kramer-type compliant surfaces. Part 2. Flow-induced surface instabilities. J Fluid Mech 1986;170:188–232.
[27] Ehrenstein U, Koch W. Three dimensional wavelike equilibrium states in plane Poiseuille's flow. J Fluid Mech 1989;228:111–48.
[28] ADINA theory and modelling guide, vol. 1–3. ADINA R&D Inc.; 2003.
[29] Bathe KJ. The finite element procedures. Englewood Cliffs, NJ: Prentice-Hall Inc.; 1996.
[30] Bathe KJ, Zhang H. Finite element development for general fluid flows with structural interactions. Int J Numer Meth Eng 2004;60:213–32.
[31] Luo XY, Cai ZX, Li WG, Pedley TJ. The cascade structure of linear stability in collapsible channel flows. J Fluid Mech [submitted for publication].